Food Analytical Methods
https://doi.org/10.1007/s12161-019-01464-0

Near Infrared Hyperspectral Imaging for White Maize Classification According to Grading Regulations

Kate Sendin[1] · Marena Manley[1] · Vincent Baeten[2] · Juan Antonio Fernández Pierna[2] · Paul J. Williams[1]

Received: 31 October 2018 / Accepted: 4 February 2019

Abstract

Near infrared hyperspectral imaging with multivariate image analysis was evaluated for its potential to grade whole white maize kernels. The study was based on grading regulations stipulated in South African legislation and aimed to provide an alternative to the tedious and subjective manual methods currently used. The types of undesirable materials regarded were divided into 13 classes and imaged using a hyperspectral imaging system (1118–2425 nm). Two approaches to data analysis, pixel-wise and object-wise, were investigated using principal component analysis (PCA) and partial least squares discriminant analysis (PLS-DA) modelling. Two-way classification models distinguished sound white maize from each type of undesirable material and were validated with independent image datasets. The pixel-wise PLS-DA demonstrated a high occurrence of errors (63–99% classification accuracy). The object-wise PLS-DA models yielded superior results, achieving 100% classification accuracy in 8 of the 13 models, with the remaining 5 incurring only one error each (98% classification accuracy). The overall classification accuracy achieved over the total 804 kernels/objects was 99.4%. Important spectral features were highlighted around 1219 and 1476 nm (associated with starch), 1941 nm (associated with moisture) and 2117 nm (associated with protein). An object-wise approach demonstrated good performance for distinguishing between the sound maize class and common grading defects and provided a classification for single, whole maize kernels, as would be conducted during the current manual grading methods. For industry implementation, this system may be simplified to a multispectral system for reduced cost and higher throughput.

Keywords Near infrared hyperspectral imaging · Chemometrics · Multivariate image analysis · Classification · Maize · Grading

Introduction

Maize, an important cereal crop, is a staple food throughout Africa, and in many other parts of the world, such as Latin America and Asia (Johnson 2000). Maize grading is a crucial and critical process, as the grade has an influence on the production and quality of the final product, and determines the market value (Serna-Saldivar 2010). The main aim of grading is thus to facilitate fair commercialisation of maize and to provide information related to quality for further storage and processing. This method is extremely labour intensive and can be considered subjective as it is assumed that the appearance of grain is related to chemical composition, functionality and optimum end use (Serna-Saldivar 2010). The current grading standards largely relate to storage issues rather than end-use factors (Johnson 2000). In South Africa, a very simple manual grading method is followed where a sample (150 g minimum) is taken and both sides of each maize kernel are visually inspected to detect any content other than sound (healthy) white maize, such as defective grain or foreign material (Department of Agriculture 2009). Undesirable materials, within each defective category, are weighed and referenced to maximum levels stipulated.

Considering the importance of accurately determining maize grade, an objective method must be developed that will recognise a wide range of defective and foreign materials important to farmers, traders and millers. Spectral imaging has been identified as a potential alternative to the current visual inspection methods (Gowen et al. 2007; Amigo et al. 2013). Hyperspectral imaging has been used in many food and agricultural applications, including studies on a wide range of cereal commodities and properties (Caporaso et al. 2018a;

✉ Paul J. Williams
pauljw@sun.ac.za

[1] Department of Food Science, Stellenbosch University Private Bag X1, Stellenbosch 7602, South Africa

[2] Food and Feed Quality Unit, Valorisation of Agricultural Products Department, Walloon Agricultural Research Centre (CRA-W), Gembloux, Belgium

Published online: 13 April 2019

Sendin et al. 2018b). These include numerous studies of maize, including hardness prediction (McGoverin and Manley 2012; Manley et al. 2011; Williams et al. 2009), chemical content prediction (Cogdill et al. 2004; Weinstock et al. 2006; Vermeulen et al. 2017b), variety identification (Wang et al. 2015) and fungal detection (Del Fiore et al. 2010; Williams et al. 2012; Vermeulen et al. 2017a). It has also been applied in the quality and safety evaluation of wheat (Mahesh et al. 2015; Manley et al. 2011; Singh et al. 2010), rice (Del Fiore et al. 2010; Wang et al. 2014), fonio (Baeten et al. 2010) and sorghum and barley (McGoverin et al. 2011).

Spectral imaging integrates conventional imaging and spectroscopy to attain both spatial and spectral information from the sample (Gowen et al. 2007; Dale et al. 2013). A spectral image comprises numerous adjacent wavelengths for each spatial point of the object, where each pixel in the image contains the spectrum at that exact point, in turn giving an indication of the chemical composition for each pixel in the image (Burger and Geladi 2006). It is thus highly suited for the study of cereal products, which show high variability in physical properties and chemical composition within and between kernels. Multispectral imaging conducted using a commercial instrument operating predominantly in the visible range (19 spectral points ranging 375–970 nm) has been used to classify the same maize grading categories with promising results (Sendin et al. 2018a). Of the 13 classes of undesirable material, 8 were classified perfectly (100%) using an object-wise approach, with classification accuracies of the remaining classes ranging 83 to 97%. However, the near infrared region should have superior capability to the visible region for detecting chemical differences in biomaterials, such as maize, due to the interaction with major X–H bonds (e.g. O–H, C–H and N–H). Furthermore, the spectral resolution offered by hyperspectral imaging in comparison with other forms of spectral imaging (i.e. multispectral imaging) allows for more in-depth investigation during data analysis which could lead to more accurate classification results in new research applications, where the best separation between classes is achieved at specific wavelengths. Once this in-depth investigation has been conducted using hyperspectral imaging, one may choose to revert to a custom-built multispectral system utilising a handful of the most significant wavelengths for the specific application.

In hyperspectral image analysis, all pixels in an image are typically considered individually. Some applications are better suited for an object-wise approach as first proposed by Burger and Geladi (2006) and later enhanced by Kucheryavskiy (2013). In this approach, the average spectrum of all pixels in an object, such as a kernel, is used during modelling. This is an appropriate approach when emulating manual grading, as whole maize kernels must be identified as either sound or defective, and each kernel should thus be observed as the lowest unit of measurement. The advantages of this approach have been demonstrated in both quantification (Caporaso et al. 2018b) and classification (Williams and Kucheryavskiy 2016) applications.

The aim of this study was to evaluate the capability of NIR hyperspectral imaging and determine the key wavebands for separating sound white maize kernels from common undesirable material types encountered in the South African maize industry. Two approaches to data analysis, namely pixel-wise and object-wise data analysis, were utilised and compared.

Materials and Methods

Samples

Maize kernels and undesirable materials were obtained from the Southern African Grain Laboratory (SAGL, Pretoria, South Africa) and were graded visually by expert graders according to South African grading regulations (Act, 2009). Of the 19 defects stipulated in the grading regulation, 13 were evaluated during this study since these were prevalent during the 2015 season. The graders provided all defected kernels, which resulted in 30 kernels per class to be included for both unique calibration and validation sample sets (60 of each class in total), with two exceptions, where 24 pinked kernels were used in each set due to limited availability and 60 screenings (i.e. broken kernels) pieces due to their small size. Subsequently, ca. 1560 samples were used in total (13 two-way analyses of 30 sound and 30 defect kernels plus independent validation sets). These 13 most prolific undesirable materials were distinguished as defective classes from the sound maize class (Fig. 1). Classes included defective white maize (heat damage, water damage, rodent damage, screenings/broken kernels, *Fusarium* fungal damage and *Diplodia* fungal damage); pinked white maize; other colour maize (i.e. yellow maize); and foreign matter (wheat, soy, sunflower seeds, sorghum and maize plant material).

NIR Hyperspectral System

Hyperspectral images were acquired using a Burgermetrics SIA system (Riga, Latvia) installed at the Walloon Agricultural Research Center (CRA-W, Belgium) that utilised a Xenics short wave infrared (SWIR) XEVA camera with an ImSpector N25E spectrograph and mercury–cadmium–telluride (HgCdTe) detector (SPECIM Ltd., Oulu, Finland). The samples were carried on a conveyer belt at a speed of 1.2 mm/s, during image acquisition on the pushbroom instrument. The system was controlled with the HyperPro software (BurgerMetrics SIA, Riga, Latvia). Individual images were acquired within a spectral range of 1118 to 2425 nm with 6.3 nm spectral resolution between the 209 spectral points. The frame rate was 100 Hz and the exposure time ranged from 0.8 to 1.2 ms. The exposure time was adjusted according to a pre-defined profile in order to be within the limits to acquire a correct image. This changed as light intensity varied with

Fig. 1 Digital image of (a) sound white maize and the 13 undesirable materials, i.e. (b) *Fusarium* damage, (c) *Diplodia* damage, (d) pinked maize, (e) water damage, (f) rodent damage, (g) heat damage, (h) plant material, (i) screenings, (j) wheat, (k) sorghum, (l) soy, (m) sunflower and (n) yellow maize

time. Images were 320 pixels wide, with a varying length of ca. 400 pixels. White and dark references were captured prior to each sample image and were subsequently used for image correction and calibration. A 100% reflectance standard (white ceramic tile) was used for the white reference, and the shutter was closed for the dark.

Image Acquisition

For the calibration set, images of each of the 13 undesirable material classes and the sound maize kernels were captured. These data sets consisted of 30 kernels/objects of a single class, with the exception of pinked kernels (24 kernels) and screenings (60 small pieces). To accurately emulate current grading practices, the classes of maize kernels (sound maize, *Fusarium* damage, *Diplodia* damage, water damage, heat damage, rodent damage and yellow maize) were first imaged with the kernels' germ facing upwards (toward the camera) and a second time with the germ facing downwards (away from the camera). Thus, the germ-up and germ-down oriented versions of the images consisted of the same kernels in the same positions. The foreign matter classes (plant material, wheat, sorghum, soy and sunflower seeds) were only imaged once, as the foreign matter often had no obvious germ. The independent validation image datasets were acquired in the same manner on new sets of kernels and objects (same number as in calibration set) for each of the 13 undesirable material classes.

Hyperspectral Image Analysis

Image correction, segmentation, spectral information extraction and multivariate data analysis were carried out using the Evince v.2.7.0 (Prediktera, Umeå, Sweden) spectral image analysis software package. The germ-up and germ-down images for each two-way analysis pair (sound kernels and undesirable materials) were mosaicked, to give a single image dataset containing a mosaic of four images. Each image mosaic was analysed individually.

Principal Component Analysis

The image calibration and correction from reflectance to pseudo-absorbance was done automatically in the Evince software package according to Eq. 1.

$$I_{\lambda,n} = -\log_{10}\left[\left(\frac{S_{\lambda,n}-B_{\lambda,n}}{W_{\lambda,n}-B_{\lambda,n}}\right)\right] \quad (1)$$

where

n = pixel index variable ($n = 1 \ldots N$) of the reorganised hypercube
$I_{\lambda,\,n}$ = standardised absorbance intensity, pixel n, at wavelength λ
$S_{\lambda,\,n}$ = Sample image, pixel n, at wavelength λ
$B_{\lambda,\,n}$ = dark reference image, pixel n, at wavelength λ
$W_{\lambda,\,n}$ = white reference image, pixel n, at wavelength λ

The mean-centred absorbance mosaic images were unfolded, whereby the three-dimensional spectral hypercube was unfolded to a two-dimensional matrix, with rows corresponding to pixels and columns to wavebands. Principal component analysis (PCA) was applied, and the spectral data from each pixel was decomposed into matrices of scores (**T**) and loadings (**P**). The score matrix for each principal component (PC) was refolded to give a score image, which visualises the main source of variation accounted by respective PCs by shading pixels with closely related spectral responses similarly. A score plot was also generated, where similar pixels are plotted close together, often referred to as clusters.

Image segmentation was performed to remove the background (i.e. conveyor belt without material), leaving only the sample data (white maize kernels and undesirable

materials). The score images and score plots of PC1 to PC3 were used to find pixels associated with either the sample or the background. Furthermore, other unwanted pixels, e.g. outliers, dead pixels, shading errors and edge effects were identified. All unwanted pixels were subsequently removed from the dataset (Esbensen and Geladi 1989). The cleaned images were used in subsequent analysis.

PCA was recalculated with additional components (up to 6) to examine the qualitative difference between sound white maize and the various undesirable material classes. Data were analysed with both pixel-wise and object-wise approaches, where the average spectrum for all pixels in each kernel was calculated as the basis for classification in the object-wise approach, and PCA (and later PLS-DA) were applied to the averaged spectra (Kucheryavskiy 2013). Pre-treatments were evaluated using the cross-validated coefficient of determination (Q2) and visual inspection of the score image and score plot. Pre-treatments yielding the highest Q2 and best separation in the score plots were selected for further analyses. Savitzky-Golay transformation (2nd order polynomial, 1st derivative, 15 points) and standard normal variate (SNV) transformation were applied to the data (Barnes et al. 1989; Savitzky and Golay 1964). In addition, the noisy wavelengths 2218 to 2425 nm were removed.

Partial Least Squares Discriminant Analysis

Partial least squares discriminant analysis (PLS-DA) models were calculated to distinguish between two classes, namely sound and each of the respective undesirable materials. As the purpose of this study is to distinguish sound maize from defective kernels of each of the 13 different categories, it is regarded as a discrimination problem, not an authentication one. PLS-DA is a technique for dimension reduction and discrimination based on conventional PLS regression; however, class membership is to be predicted (Barker and Rayens 2003). A binary dummy matrix (**Y**) of the two classes, namely sound class and undesirable material class, is related to the calibration set spectral data (**X**). PLS is calculated, and the validation set is tested by assigning class membership. Pixel-wise and object-wise PLS-DA models were calculated on the calibration image data, with partial even spread cross-validation for the pixel-wise models, as the number of pixels was large, and full cross-validation for the object-wise models. The mean spectrum of all the pixels in a kernel was used to obtain an object during object-wise analyses. The PLS-DA models were applied to the independent validation image dataset, pixels or objects were predicted, and a classification image was generated. The pixels or objects were shaded as blue (predicted as sound) or green (predicted as undesirable material), and this image was referred to as the unaltered classification image in later sections.

External validation of the germ-up and germ-down image pairs was conducted to determine each kernel's overall classification, according to Table 1. For food safety reasons, if any kernel is classified as undesirable on either one or two sides, it is immediately flagged as an undesirable material. Once the unaltered classification image was generated, the correct and incorrect classifications were totalled with reference to the kernels' true classes (as determined by expert graders). The kernels were shaded according to correct and incorrect classifications, and this image was referred to as the overall classification image. A correctly classified sound kernel corresponds to a true negative, and a correctly classified undesirable material corresponds to a true positive. Conversely, a false positive occurred when a sound kernel was incorrectly classified as undesirable material, and a false negative was when an undesirable material was incorrectly classified sound.

All correct overall classifications (true positives and true negatives) formed part of the correct classification accuracy (%). Incorrect classifications were either false positives or false negatives, forming part of the false positive error (%) or false negative error (%), respectively. Classification accuracy, false positive error and false negative error were calculated according to Eqs. 2, 3 and 4, respectively.

$$\text{Classification accuracy } (\%) = \frac{\text{Correct defect} + \text{correct sound}}{\text{Total}} \times 100\% \quad (2)$$

$$\text{False positive error } (\%) = \frac{\text{False positives}}{\text{Total}} \times 100\% \quad (3)$$

$$\text{False negative error } (\%) = \frac{\text{False negatives}}{\text{Total}} \times 100\% \quad (4)$$

where

Correct defect	= correctly classified class 'defect' kernels
Correct sound	= correctly classified class 'sound' kernels
False positives	= 'sound' class kernels incorrectly classified 'defect' class
False negatives	= 'defect' class kernels incorrectly classified 'sound' class
Total	= sum of 'defect' and 'sound' kernels

Sensitivity and specificity were calculated according to Eqs. 5 and 6, respectively. The sensitivity describes the probability that undesirable materials will be detected and correctly classified and is sometimes described as the true positive rate. Specificity is the probability that a sound kernel will be classified correctly, also known as the true negative rate.

$$\text{Sensitivity } (\%) = \frac{\text{Correct defect}}{\text{Total defect}} \times 100\% \quad (5)$$

Table 1 Method used to determine the classification result of a kernel/object

True class	Germ-up	Germ-down	Overall	Result	
Sound (negative result)	Sound	Sound	Sound	✓	True negative
	Sound	Defect	Defect	✗	False positive
	Defect	Sound	Defect	✗	False positive
	Defect	Defect	Defect	✗	False positive
Defect (positive result)	Sound	Sound	Sound	✗	False negative
	Sound	Defect	Defect	✓	True positive
	Defect	Sound	Defect	✓	True positive
	Defect	Defect	Defect	✓	True positive

$$\text{Specificity}\ (\%) = \frac{\text{Correct sound}}{\text{Total sound}} \times 100\% \quad (6)$$

where

Correct defect = correctly classified class 'defect' kernels
Correct sound = correctly classified class 'sound' kernels
Total defect = total 'defect' kernels (correct defect + false negatives)
Total sound = total 'sound' kernels (correct sound + false positives)

Results and Discussion

Spectral Analysis

The raw average pseudo-absorbance spectra (1118 to 2211 nm) of the sound white maize, defective white maize and pinked white maize classes are given in Fig. 2, and sound white maize, yellow maize and the foreign matter classes are shown in Fig. 3. The spectra of the classes tend to follow a similar shape. The only exception was the first section of the sunflower seeds' spectrum. This is likely due to the seed being contained within an outer black husk through which the NIR wavelengths could not fully penetrate (Pérez-Vich et al. 1998). Thus, information regarding the absorption characteristics of the husk were measured and not the inner sunflower seed. The outer husk, comprising mostly of cellulose (ca. 48%), hemicellulose (ca. 35%) and lignin (ca. 17%), has a very different chemical signature to the other starch-rich cereal commodities (Demirbaş 2002).

The differences in intensity exhibited between the spectra of the classes cannot be solely attributed to the internal chemical composition of the kernels directly. Instead, physical effects such as scattering likely contributed substantially to the varying intensities. Furthermore, direct interpretation of heterogeneous samples like whole maize kernels are difficult, as the spectra contain the combined information from all kernel components. However, general trends were observed. Four main absorption bands in the spectra of the 14 classes were exhibited around 1219, 1476, 1941 and 2117 nm. The peaks at 1219 (C–H stretch, second overtone) and 1476 nm (O–H stretch, first overtone) indicate variation in the starch composition of the endosperm (Delwiche and Hareland 2004; Manley et al. 2009). The broad peak around 1476 nm also has a contribution from moisture at approximately 1430 nm. A clear moisture peak was apparent due to an O–H stretch around 1941 nm (Manley et al. 2009) and the peak present around 2117 nm relates to amino acids (N–H stretch, first overtone), and thus protein content (Fernández-Ibañez et al. 2009).

Multivariate Data Analysis

Principal Component Analysis

The class heat damage and screenings (broken kernels) vs. sound class are used to illustrate the PCA results, as given in Figs. 4 and 5 for the pixel-wise analyses and Figs. 6 and 7 for the object-wise analyses. Note that the score plots (a) are shaded according to density of points, while the score images (b) are shaded according to scores value, where blue is negative and red is positive.

During the pixel-wise PCA analyses, the spectrum from each pixel in the cleaned image is included during modelling. The PC1 vs. PC2 score plot showed a major overlap of the two classes, where the two semi-defined clusters did not relate to the two classes but were uniformly associated with both (Figs. 4a and 5a). The variance accounted by PC1 (ca. 80% SS) was likely due to variation within the kernels and their anatomical kernel components. The cluster to the left of the PC score plot (Figs. 4a and 5a) is associated with negative scores in PC1 and is related to the pixels shaded in blue and green tones on the PC1 score images (Figs. 4b and 5b). These regions of the kernel are anatomically known as the soft (inner regions) and hard endosperm (outer regions) (Fox and Manley 2009). These parts of the kernel consist mainly of starch. The cluster to the right of the PC score plot is associated with positive scores in PC1, and these pixels are shown in red and known as

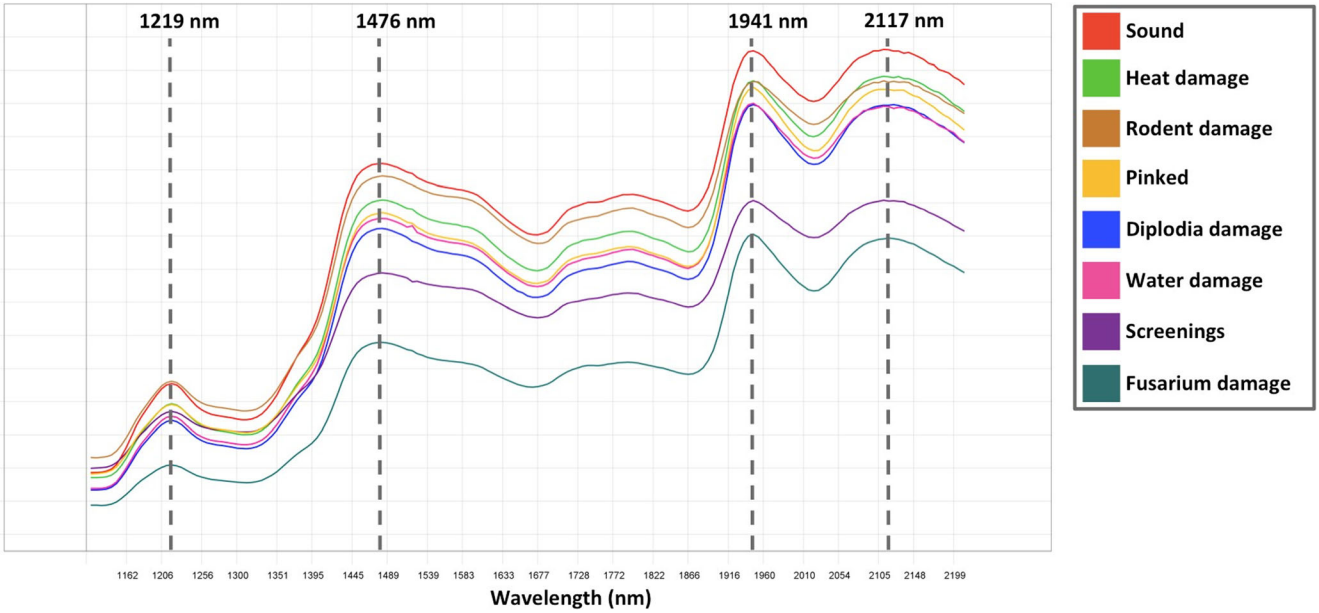

Fig. 2 Unprocessed average absorbance NIR spectra for sound white maize; white maize defects (heat damage, rodent damage, *Diplodia* damage, water damage, screenings and *Fusarium* damage); and pinked white maize

the germ, which has higher lipid content. Thus, the clusters that appeared in the direction of PC1 in the score plots were found to correspond with the differences in chemical content of the anatomical components of the kernels regardless of the kernel's class. Furthermore, there is an observable difference in overall shading of the germ-up and germ-down images (Figs. 4b and 5b), again exhibiting variation attributed to anatomical differences and not difference between classes. For the maize classes heat damage (Fig. 4), water damage, rodent damage, yellow maize, screenings (Fig. 5), *Fusarium* damage, *Diplodia* damage and pinked kernels, the majority of variance in PC2 continued to arise from within individual kernels as opposed to between the classes. PC3 (not shown) accounted for the difference in germ orientation, where a cluster appeared in the score plot related to the large germ appearing on the germ-up oriented kernels. The foreign matter classes exhibited differences between the two classes in the initial PCs. Wheat, sorghum and soy exhibited similar variance within kernels in PC1, but exhibited clear separation of classes from PC2 onward. This was likely due to less similarity between chemical components of these cereal commodities. Sunflower seeds (which included the outer husk) and plant

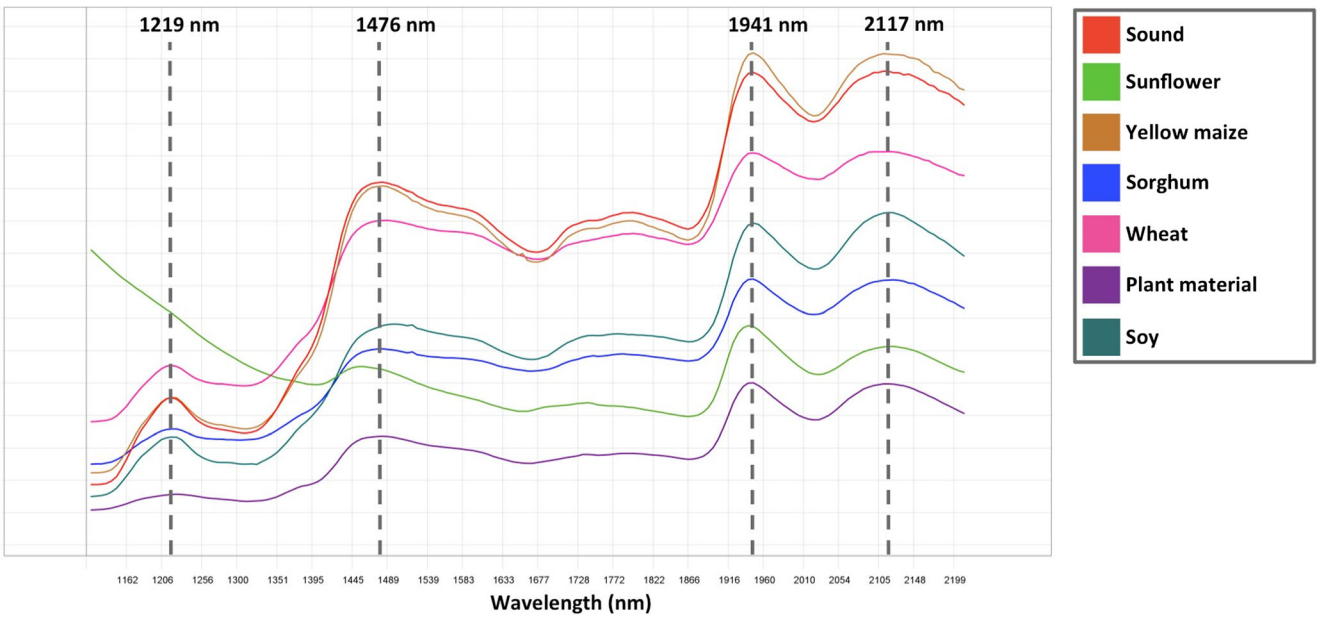

Fig. 3 Unprocessed average absorbance NIR spectra for sound white maize; yellow maize; and foreign matter (sunflower seeds, sorghum, wheat, plant material and soy)

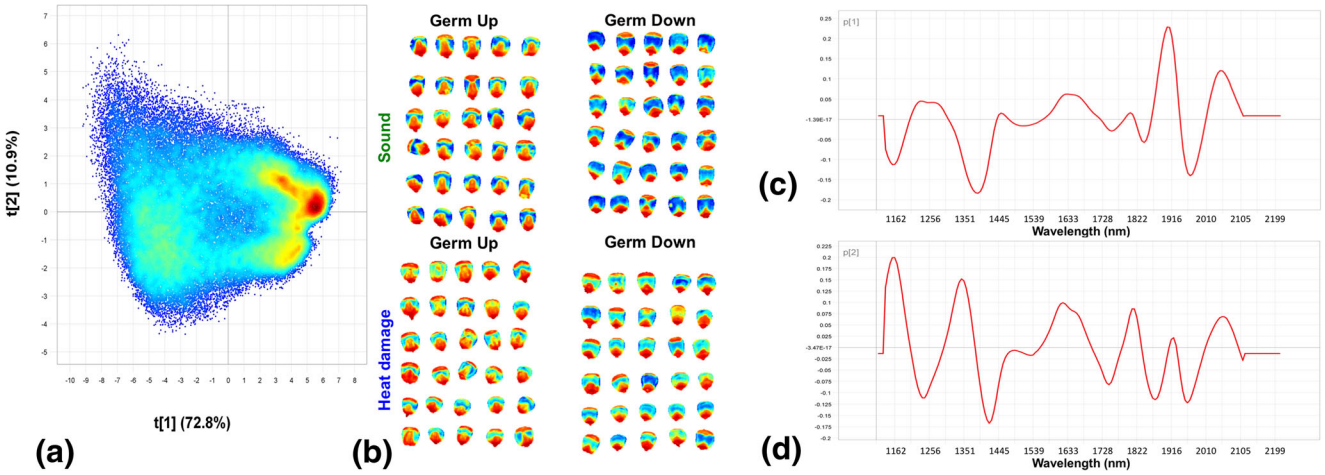

Fig. 4 Pixel-wise PCA analysis of heat damage class vs. sound class (Savitzky-Golay (2nd order polynomial, 1st derivative, 15 points) and SNV transformations). Scores given as **a** PCA score plot of PC1 (72.8% SS) vs. PC2 (10.9% SS) and **b** PCA score image (PC1). Loading line plots given for **c** PC1 and **d** PC2. SS, sum of squares; SNV, standard normal variate; PCA, principal component analysis; PC, principal component

material had extremely different chemical surface characteristics to maize, likely due to their high cellulose contents, and thus were clearly separated from sound maize in PC1. This type of separation should have ideally occurred in more of the 13 analyses, but was prevented due to similarities between classes. Overall, the overwhelming lack of separation between sound maize and most undesirable materials emphasises the need to investigate an object-wise approach, where these internal variances were excluded by averaging the spectra of all individual pixel spectra in a single kernel.

The object-wise PCA analyses revealed distinctions in the score plot between the classes in PC1 that were not seen in the pixel-wise results. The PC1 vs. PC2 score plots (Figs. 6a and 7a) of most classes show a clear separation of scores between the sound (green) and undesirable material (blue) objects. It seems that by eliminating the variation within the kernels and their anatomical kernel components through the calculation of average spectra, the more subtle overall variation between the classes may be expressed in the earlier PCs during object-wise analysis. Generally, the points on the score plots were separated predominantly in the direction of PC1, as illustrated by heat damage (Fig. 6) and screenings (Fig. 7a). PC1 accounted for the differences between the two classes, while the variance explained in PC2 may relate to intra-class separation, such as endosperm hardness effects (Manley et al. 2009).

All analyses projected the sound class with negative scores and the undesirable material class with positive scores. Although assigned arbitrarily, scores values indicate which class will be associated with high absorbance of wavelengths with either positive or negative loadings. The loading line plots of PC1 and PC2 (Figs. 4c, 5c, 6c, 7c and 4d, 5d, 6d, 7d) were similar throughout the classes in both the pixel-wise

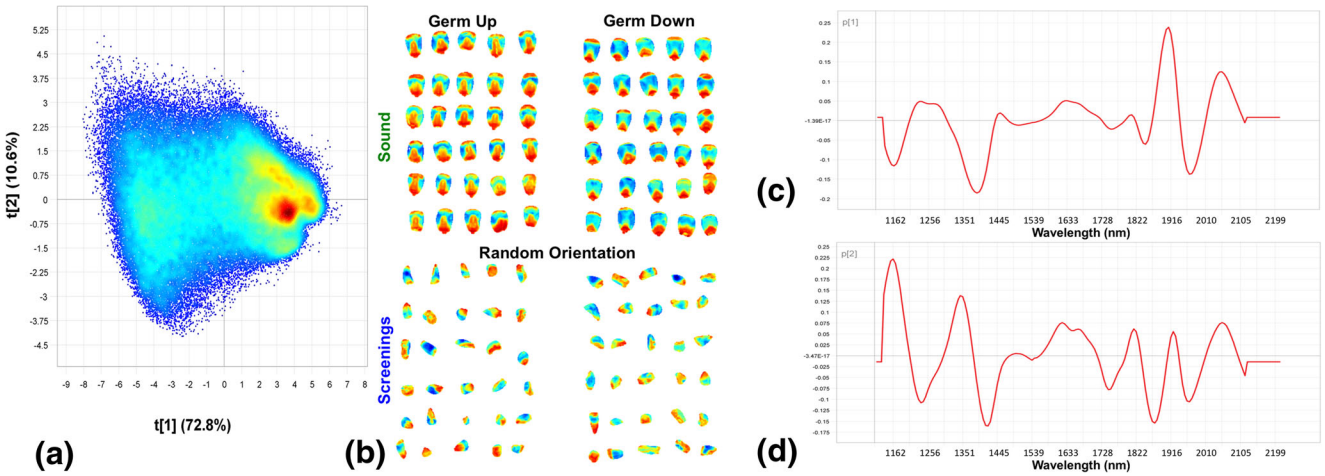

Fig. 5 Pixel-wise PCA analysis of screenings class vs. sound class (Savitzky-Golay (2nd order polynomial, 1st derivative, 15 points) and SNV transformations). Scores given as **a** PCA score plot of PC1 (72.8% SS) vs. PC2 (10.6% SS) and **b** PCA score image (PC1). Loading line plots given for **c** PC1 and **d** PC2

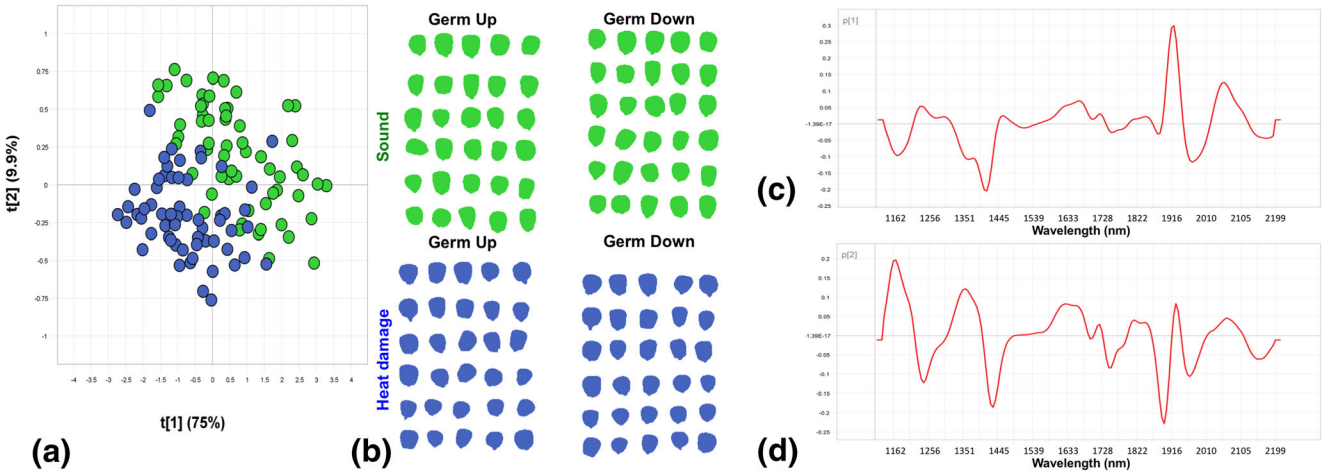

Fig. 6 Object-wise PCA analysis of heat damage class vs. sound class (Savitzky-Golay (2nd order polynomial, 1st derivative, 15 points) and SNV transformations). **a** PCA score plot of PC1 (75% SS) vs. PC2 (9.9% SS). **b** Classes of sound (green) and heat damaged (blue) objects. Loading line plots given for **c** PC1 and **d** PC2

and object-wise results. Prominent positive bands were observed in PC1 at 1231, 1275 and 1910 nm, and thus associated with the positive scores of the undesirable materials, and negative loadings at 2045 nm, and 1162, 1388, 1966 and 2180 nm, associated with the negative scores of the sound class. As the first derivative was calculated with the Savitzky-Golay smoothing transformation, the original sharp single peaks observed in the spectral analysis were split into two peaks, one positive and one negative. The first derivative spectrum will cross zero at the original (raw) spectrum's maximum, with the two peaks either side exhibiting maxima where the original peak had its maximum gradients (Brereton 2003). The negative and positive pairs at ca. 1162 and 1275 nm, respectively, are likely related to the C–H stretch second overtone for starch originally identified at ca. 1219 nm. Furthermore, there is a second unresolved positive peak between the two at ca. 1231 nm which could be paired with the negative peak at 1388 nm. This is likely also related to a C–H stretch second overtone absorption by similar groups (Osborne and Fearn 1986). Although there is a slight shoulder in this region on the original spectrum (ca. 1370 nm), it remained unresolved and overshadowed by other major bands. This emphasises the importance of inspecting both the original spectrum and loadings for key wavebands. The moisture band at ca. 1941 nm was split into the positive and negative pair at ca.1910 and 1966, respectively, while the pair at 2045 and 2180 nm is likely related to the N–H stretch first overtone related to amino acids originally at ca. 2117 nm. The last prominent peak identified in the spectral analysis was an O–H stretch first overtone related to starch at ca. 1476 nm; however, the bands appearing in the loadings at ca. 1439 and 1520 nm may be considered minor due to relatively lower loading value. This indicates that, despite starch content resulting in high absorbance, there was little difference between the samples. This band was thus not a strong driver in the separation during PCA.

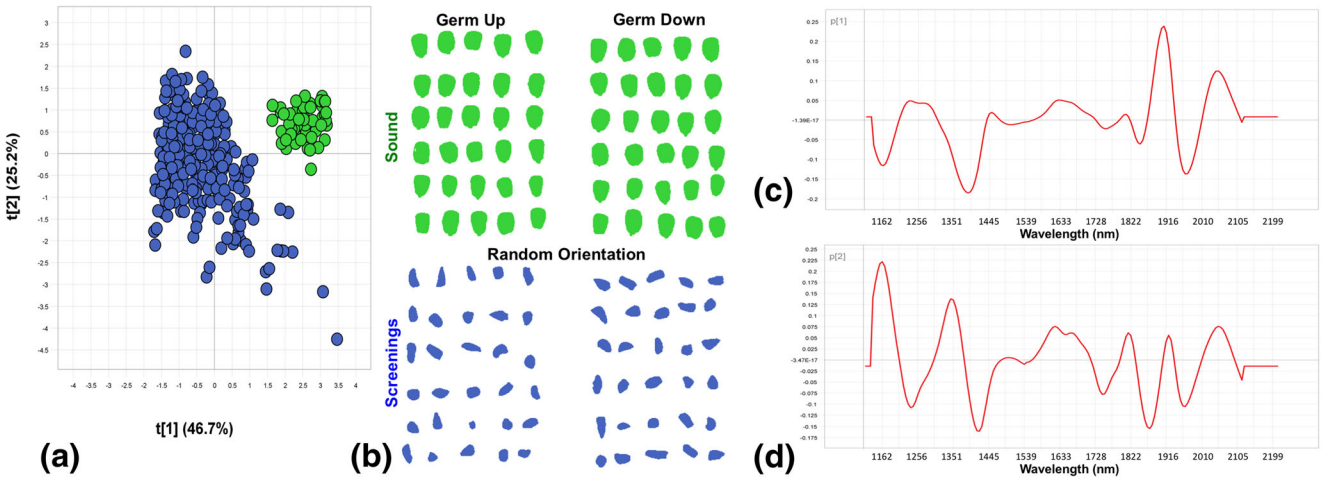

Fig. 7 Object-wise PCA analysis of screenings class vs. sound class (Savitzky-Golay (2nd order polynomial, 1st derivative, 15 points) and SNV transformations). **a** PCA score plot of PC1 (46.7% SS) vs. PC2 (25.2% SS). **b** Classes of sound (green) and screenings (blue) objects. Loading line plots given for **c** PC1 and **d** PC2

The loadings of PC2 show prominent bands at very similar points to PC1. Notably, the unresolved positive peaks around 1256 nm in PC1 separated into negative and positive peaks at ca. 1231 and 1275 nm, respectively. Some wavebands showed inverted loading values (positive changing to negative and vice versa). However, as the loading value is allocated arbitrarily, this does not greatly affect how these results should be interpreted and only indicates that in PC2 the absorbance of the waveband is associated with scores of opposite value to PC1.

Partial Least Squares Discriminant Analysis

PLS-DA was selected to determine class membership to each of the pre-defined 13 defective categories. The classification accuracy, false positive error and false negative error demonstrate the classification performance of the models when applied to an independent validation image dataset. The classifications by pixel-wise PLS-DA exhibited a large incidence of errors, with classification accuracy results varying widely between 63% (pinked white maize) and 99.7% (sunflower seeds) (Table 2). All object-wise PLS-DA models performed well (Table 3) with 8 of the 13 analyses achieving 100% classification accuracy, including *Diplodia* damage, heat damage, screenings, plant material, wheat, sorghum, soy and sunflower. The 5 remaining classes only predicted one kernel incorrectly. The classes with one false positive (sound kernel incorrectly classified as undesirable material) include *Fusarium* damage and yellow maize, and the classes with one false negative (undesirable material not detected) included water damage, rodent damage and pinked white maize kernels.

The pixel-wise PLS-DA score plots for PLS factors 1 vs. 2 for yellow maize and screenings vs. sound class are given in Figs. 8a and 9a. The score plots were indicative of the limited classification abilities of the models. Although the plots exhibit slightly clearer separations of class's pixels than in the pixel-wise PCA results, there was an overlap between majority of the points. Some separation was apparent, notably in the screenings class (Fig. 9a). In general, the separation occurred in the directions of both PLS factors 1 and 2, where the sound class was associated with the positive scores of both factors and the undesirable material class with the negative scores.

The considerable overlap of points, thus representing pixels with very similar spectral information between both classes, throughout the PLS-DA score plots was accompanied by a large number of pixels being incorrectly classified, as seen in the pixel-wise classification images (Figs. 8b and 9b). In the pixel-wise classification images, pixels cannot be related back to an exact location between sets of images in the same manner one would compare whole kernels. It was thus not possible to compare the outcomes of the germ-up and germ-down image pairs pixel by pixel. For these analyses, the results of correct and incorrect predictions were simply averaged for the sum of all pixels in the image pair. The large number of errors tended to arise in regions of the kernel that were very similar in both classes. Figure 8b demonstrates that the model appears to be unexpectedly strongly calibrated for classifying the kernel components as opposed to the classes, despite the use of a supervised method such as PLS-DA. The sound class seems to be associated with correct classification of the hard endosperm and the germ, and the soft endosperm is often misclassified. The inverse occurred for the yellow maize class, where the hard endosperm and germ were often misclassified as sound. The model was predicting endosperm hardness as opposed to white and yellow maize. Unlike wheat, which generally consists of one endosperm type, maize contains both vitreous and floury endosperm in a single kernel. A

Table 2 Results of pixel-wise PLS-DA models for the separation of sound white maize class from 13 undesirable material classes

Undesirable material	PLS factors	Classification accuracy (%)	False negatives (%)	False positives (%)	Sensitivity (%)	Specificity (%)
Fusarium damage	5	82.67	9.35	7.97	84.38	86.07
Diplodia damage	5	85.22	7.83	6.95	80.04	84.99
Water damage	4	78.78	13.17	8.05	92.45	89.19
Rodent damage	3	82.95	6.13	10.92	74.64	83.26
Heat damage	4	90.72	3.54	5.74	71.99	86.02
Screenings	3	91.58	2.85	5.57	88.77	92.54
Pinked maize	4	62.94	14.23	22.83	40.91	69.93
Yellow maize	4	75.32	9.02	15.65	90.17	96.20
Plant material	2	86.86	6.43	6.71	98.49	99.63
Wheat	4	90.87	2.09	7.04	2.38	92.80
Sorghum	5	96.04	0.26	3.70	68.68	92.80
Soy	3	99.46	0.23	0.31	83.17	89.15
Sunflower	2	99.65	0.00	0.35	77.85	73.59

Table 3 Results of object-wise PLS-DA models for the separation of sound white maize class from 13 undesirable material classes

Undesirable material	PLS factors	Classification accuracy (%)	False negatives (%)	False positives (%)	Sensitivity (%)	Specificity (%)
Fusarium damage	5	98.33	0.00	1.67	100.00	96.67
Diplodia damage	5	100.00	0.00	0.00	100.00	100.00
Water damage	4	98.33	1.67	0.00	96.67	100.00
Rodent damage	3	98.33	1.67	0.00	96.67	100.00
Heat damage	4	100.00	0.00	0.00	100.00	100.00
Screenings	3	100.00	0.00	0.00	100.00	100.00
Pinked maize	4	98.15	1.85	0.00	95.83	100.00
Yellow maize	4	98.33	0.00	1.67	100.00	96.67
Plant material	2	100.00	0.00	0.00	100.00	100.00
Wheat	4	100.00	0.00	0.00	100.00	100.00
Sorghum	5	100.00	0.00	0.00	100.00	100.00
Soy	3	100.00	0.00	0.00	100.00	100.00
Sunflower	2	100.00	0.00	0.00	100.00	100.00

kernel is not only hard or only soft, and hardness is classified by the ratio of the two as soft, intermediate and hard (Manley et al. 2009; Sendin et al. 2018b). Similar outcomes occurred in the remaining analyses, due to either substantial variation within a kernel's components (such as endosperm hardness) which were more distinct than differences between classes, or when a defect did not invade all particular regions of a kernel and leaving particular regions seemingly sound and thus similar in both classes. The classification of wheat was the poorest outcome of all analyses. The classification accuracy was not as severely affected (90.87%) as the much smaller wheat kernels contributed very few pixels toward the averaged value relative to the large maize kernels. However, the incredibly low sensitivity of the model (2.38%) reveals how poorly suited the model was for the prediction of wheat content in a maize sample. The similarities in chemical composition between maize and wheat (e.g. high starch content) could have affected the separation of the two commodities in the NIR region and could potentially be better predicted based on differences in the visible region.

The broad range of classification accuracies (63–99%), sensitivity (2–98%) and specificity (70–99%) (Table 2)

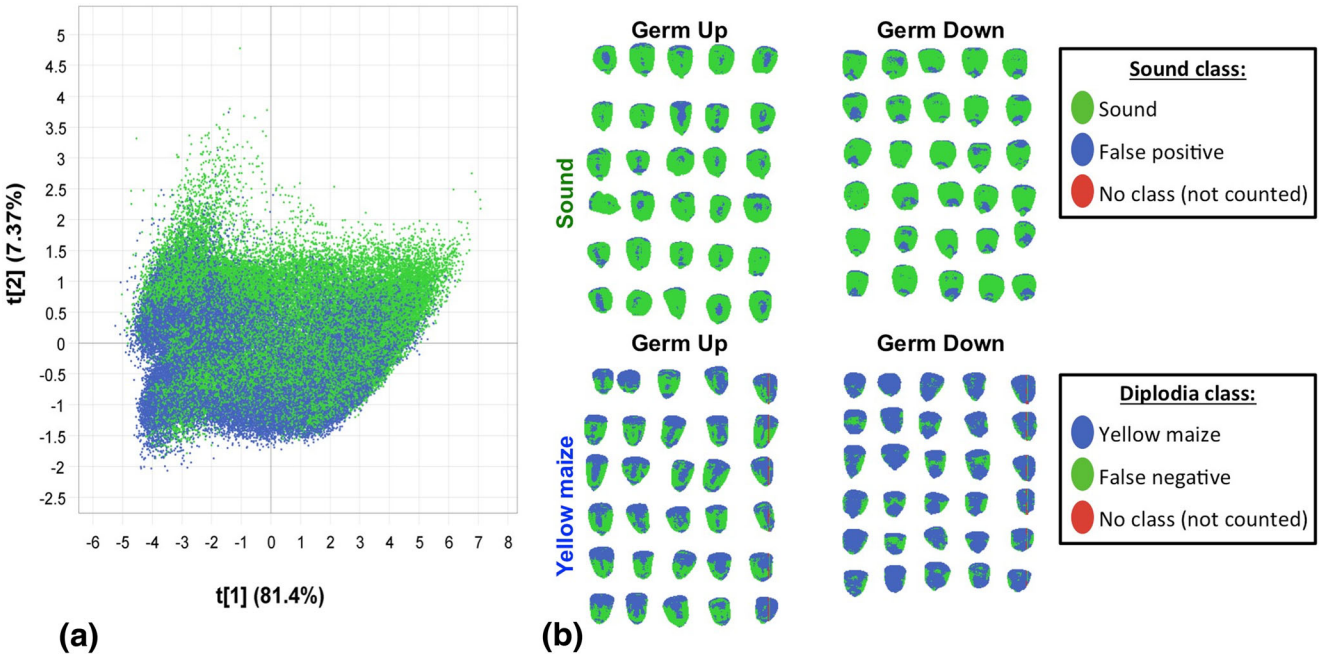

Fig. 8 Pixel-wise PLS-DA classification of yellow maize class vs. sound class (90.72% classification accuracy). **a** PLS-DA score plot of PLS factor 1 (81.4% SS) vs. 2 (7.37% SS). **b** Classification image

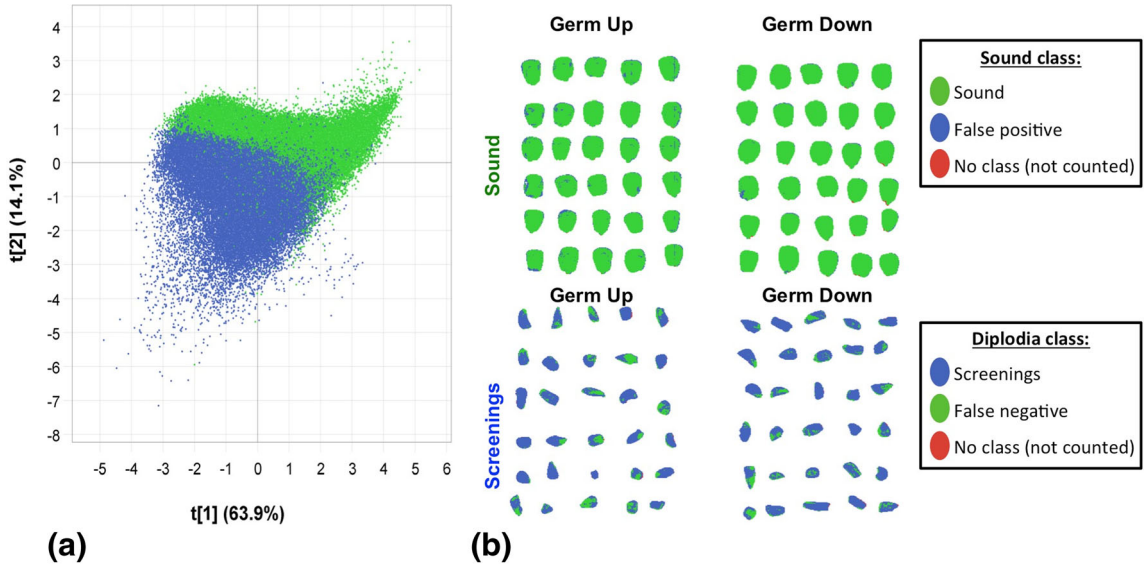

Fig. 9 Pixel-wise PLS-DA classification of screenings class vs. sound class (91.58% classification accuracy). **a** PLS-DA score plot of PLS factor 1 (64% SS) vs. 2 (14% SS). **b** Classification image

demonstrates the difficulty of differentiating between classes when there is a large overlap of pixels with similar chemical composition. The only class with an exceptionally high classification accuracy was sunflower seeds (99.65%), most likely due to the complete difference in spectral information because of the chemical composition of the cellulose-rich sunflower seed husks versus the starchy maize kernels.

The object-wise PLS-DA score plots for yellow maize and screenings vs. sound class are given in Figs. 10a and 11a. The score plots demonstrate little overlap between the classes, indicating improved model calibration. The score plot of the screening class (Fig. 11a) exhibited the most striking separation, with two tightly arranged clusters on either side of the PLS factor 1 axis. There was little separation in the direction of PLS factor 2. Similarly, the foreign matter classes (wheat, soy, sorghum, sunflower and plant material) and yellow maize exhibited the majority of separation in the direction of PLS factor 1, while the spread across PLS factor 2 was generally intra-class separation. The remaining maize classes, demonstrated by yellow maize (Fig. 10a), tended to show separation occurring in the direction of both PLS factors 1 and 2.

The object-wise PLS-DA analyses yielded promising results and clearly demonstrated the advantages of using an object as the lowest unit of measurement. The majority of classes were predicted perfectly, and no more than one error per two-way classification occurred in the remaining analyses. The yellow maize class (Fig. 10) demonstrated the importance of capturing images of the kernels in both the germ-up and germ-down orientation. In the germ-up image, 2 of the 30 pinked kernels were misclassified. However, when the kernels

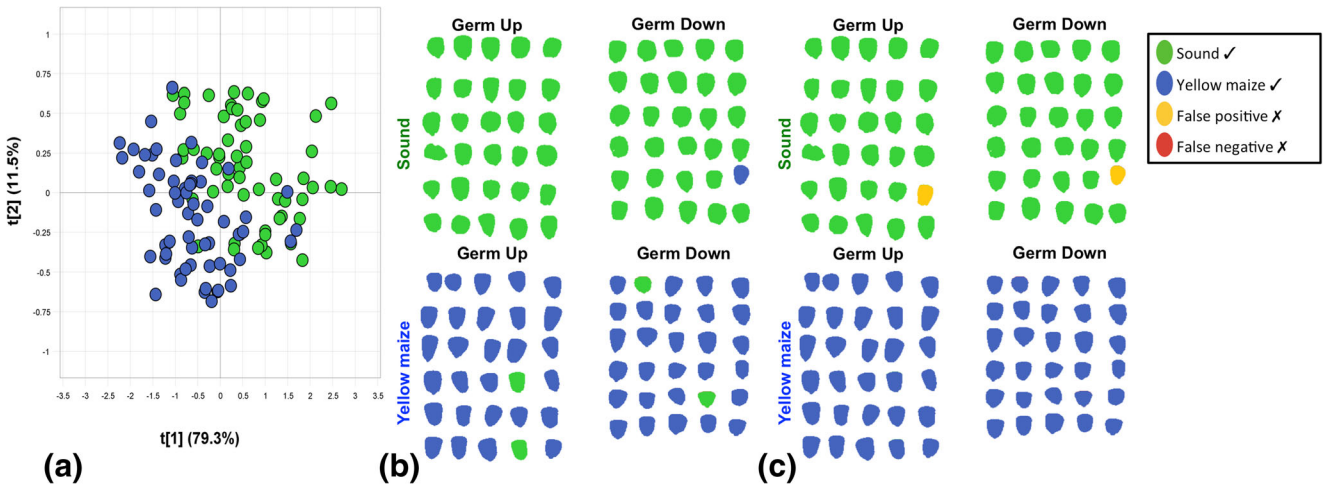

Fig. 10 Object-wise PLS-DA classification of yellow maize class vs. sound class (100% classification accuracy). **a** PLS-DA score plot of PLS factor 1 (79.3% SS) vs. 2 (11.5% SS), **b** unaltered classification image (predictions only) and **c** overall classification image (predictions evaluated according to correct class)

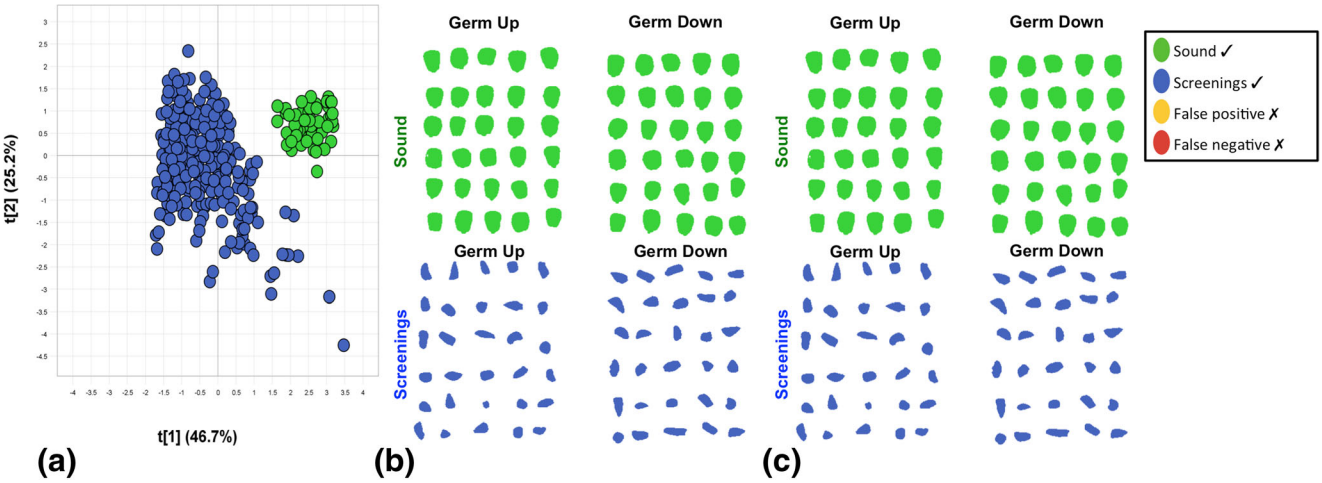

Fig. 11 Object-wise PLS-DA classification of screenings class vs. sound class (100% classification accuracy). **a** PLS-DA score plot PLS factor 1 (47% SS) vs. 2 (25% SS), **b** unaltered classification image (predictions only) and **c** overall classification image (predictions evaluated according to correct class)

were turned over, the 2 previously misclassified kernels were correctly identified as defective, while 2 different kernels were misclassified. Thus, all 30 kernels were flagged as undesirable on at least one side and no false negatives occurred. Similar instances occurred during the analysis of the *Diplodia* and pinked maize classes.

The sensitivity and specificity were all above 95%, with classification accuracies ranging 98–100%. Overall, the sensitivity and specificity of the object-wise models were considerably higher than their pixel-wise counterparts. This demonstrates the ability of an object-wise approach to see beyond the noise of class overlap and find meaningful differences between two classes for the purpose of classification.

Conclusion

Hyperspectral imaging was successfully used to separate sound white maize from the 13 major classes of undesirable materials encountered during industry grading practices. The pixel-wise PCA results were influenced by large heterogeneity of the kernels, which overshadowed the less prominent differences in spectral information between the closely related classes. The main sources of variance were due to differences within the kernels (the various anatomical kernel components) and not due to differences between the classes. The pixel-wise PLS-DA analyses yielded classifications that were not sufficiently accurate for industry implementation. They included a large number of errors with classification accuracies ranging 63–99.7%. The object-wise approach eliminated any possibility of detecting variance within a kernel by using the whole kernel as the smallest unit of measurement. By calculating an average spectrum per kernel, the object-wise PCA analysis achieved reasonable separation of the classes. The object-wise PLS-DA analyses were successful in achieving accurate classification of both classes. Of the 13 two-way analyses (ca. 30 validation objects per class), 8 achieved perfect results, and the remaining 5 analyses contained only 1 error each per analysis of ca. 60 kernels (1.6% error). Thus, of the 804 kernels/objects imaged, 799 were correctly classified, giving an overall classification accuracy of 99.4%. As the models were independently validated, the results have demonstrated the accuracy of the model calibrations. Hyperspectral imaging paired with object-wise multivariate data analysis was shown to be highly suitable for separating sound white maize from common undesirable materials and has a promising future in cereal grading applications. For continued routine analysis in this application, the wavelengths 1219 and 1476 nm (associated with starch), 1941 nm (associated with moisture) and 2117 nm (associated with protein) are suggested for developing a rapid multispectral instrument.

Acknowledgments The authors thank Nicaise Kayoka from CRA-W for his support in the acquisition and pre-processing of the NIR hyperspectral images.

Funding This work is based on the research supported in part by the National Research Foundation of South Africa (grant numbers 94031 and 95343) and The Maize Trust of South Africa.

Compliance with Ethical Standards

Conflict of Interest The authors declare that they have no conflict of interest.

Ethical Approval This article does not contain any studies with human participants or animals performed by any of the authors.

Informed Consent Not applicable.

References

Amigo, J. M., Martí, I. & Gowen, A. (2013). Hyperspectral imaging and chemometrics: a perfect combination for the analysis of food

structure, composition and quality. In: *Data handling in science and technology.* Pp. 343–370. Amsterdam: Elsevier Science

Baeten V, Fernandez Pierna JA, Vermeulen P, Dardenne P (2010) NIR hyperspectral imaging methods for quality and safety control of food and feed products: contributions to four European projects. NIR News 21(6):10–13

Barker M, Rayens W (2003) Partial least squares for discrimination. J Chemometrics: J Chemometrics Soc 17(3):166–173

Barnes RJ, Dhanoa MS, Lister SJ (1989) Standard normal variate transformation and de-trending of near-infrared diffuse reflectance spectra. Appl Spectrosc 43(5):772–777

Brereton, R. G. (2003). Signal Processing. In: *Chemometrics: data analysis for the laboratory and chemical plant*. Pp. 119–182. Chichester: John Wiley & Sons

Burger J, Geladi P (2006) Hyperspectral NIR imaging for calibration and prediction: a comparison between image and spectrometer data for studying organic and biological samples. Analyst 131(10):1152–1160

Caporaso N, Whitworth MB, Fisk ID (2018a) Near-infrared spectroscopy and hyperspectral imaging for non-destructive quality assessment of cereal grains. Appl Spectrosc Rev 53:667–687. https://doi.org/10.1080/05704928.2018.1425214

Caporaso N, Whitworth MB, Fisk ID (2018b) Protein content prediction in single wheat kernels using hyperspectral imaging. Food Chem 240:32–42

Cogdill RP, Hurburgh CR, Rippke GR, Bajic SJ, Jones RW, McClelland JF, Jensen TC, Liu J (2004) Single-kernel maize analysis by near-infrared hyperspectral imaging. Trans ASAE 47(1):311–320

Dale LM, Thewis A, Boudry C, Rotar I, Dardenne P, Baeten V, Fernandez Pierna JA (2013) Hyperspectral imaging applications in agriculture and agro-food product quality and safety control: a review. Appl Spectrosc Rev 48(2):142–159

Del Fiore A, Reverberi M, Ricelli A, Pinzari F, Serranti S, Fabbri AA, Bonifazi G, Fanelli C (2010) Early detection of toxigenic fungi on maize by hyperspectral imaging analysis. Int J Food Microbiol 144(1):64–71

Delwiche SR, Hareland GA (2004) Detection of scab-damaged hard red spring wheat kernels by near-infrared reflectance. Cereal Chem 81(5):643–649

Demirbaş A (2002) Fuel characteristics of olive husk and walnut, hazelnut, sunflower, and almond shells. Energy Sources 24(3):215–221

Department of Agriculture (2009). Regulations relating to the grading, packing and marking of maize intended for sale in the Republic of South Africa. In: Agricultural Product Standards Act (Act No. 119 of 1990)

Esbensen K, Geladi P (1989) Strategy of multivariate image analysis (MIA). Chemom Intell Lab Syst 7(1):67–86

Fernández-Ibañez V, Soldado A, Martínez-Fernández A, De la Roza-Delgado B (2009) Application of near infrared spectroscopy for rapid detection of aflatoxin B1 in maize and barley as analytical quality assessment. Food Chem 113(2):629–634

Fox G, Manley M (2009) Hardness methods for testing maize kernels. J Agric Food Chem 57(13):5647–5657

Gowen AA, O'Donnell CP, Cullen PJ, Downey G, Frias JM (2007) Hyperspectral imaging—an emerging process analytical tool for food quality and safety control. Trends Food Sci Technol 18(12):590–598

Johnson LA (2000) The major cereal of the Americas. In: Kulp K, Ponte JG (eds) In: Handbook of cereal science and technology, revised and expanded. CRC Press, New York, pp 31–80

Kucheryavskiy S (2013) A new approach for discrimination of objects on hyperspectral images. Chemom Intell Lab Syst 120:126–135

Mahesh S, Jayas DS, Paliwal J, White NDG (2015) Comparison of partial least squares regression (PLSR) and principal components regression (PCR) methods for protein and hardness predictions using the near-infrared (NIR) hyperspectral images of bulk samples of Canadian wheat. Food Bioprocess Technol 8(1):31–40

Manley M, Williams P, Nilsson D, Geladi P (2009) Near infrared hyperspectral imaging for the evaluation of endosperm texture in whole yellow maize (Zea maize L.) kernels. J Agric Food Chem 57(19):8761–8769

Manley M, Du Toit G, Geladi P (2011) Tracking diffusion of conditioning water in single wheat kernels of different hardnesses by near infrared hyperspectral imaging. Anal Chim Acta 686(1):64–75

McGoverin C, Manley M (2012) Classification of maize kernel hardness using near infrared hyperspectral imaging. J Near Infrared Spectrosc 20:529

McGoverin CM, Engelbrecht P, Geladi P, Manley M (2011) Characterisation of non-viable whole barley, wheat and sorghum grains using near-infrared hyperspectral data and chemometrics. Anal Bioanal Chem 401:2283–2289

Osborne, B. G., & Fearn, T. (1986). Theory of near infrared spectroscopy. In: *Near infrared spectroscopy in food analysis*. Pp. 29–33. Harlow: Longman Scientific & Technical

Pérez-Vich B, Velasco L, Fernández-Martínez J (1998) Determination of seed oil content and fatty acid composition in sunflower through the analysis of intact seeds, husked seeds, meal and oil by near-infrared reflectance spectroscopy. J Am Oil Chem Soc 75(5):547–555

Savitzky A, Golay MJE (1964) Smoothing and differentiation of data by simplified least squares procedures. Anal Chem 36(8):1627–1639

Sendin K, Manley M, Williams PJ (2018a) Classification of white maize defects with multispectral imaging. Food Chem 243:311–318

Sendin K, Williams PJ, Manley M (2018b) Near infrared hyperspectral imaging in quality and safety evaluation of cereals. Crit Rev Food Sci Nutr 58(4):575–590

Serna-Saldivar, S. O. (2010). Physical properties, grading, and speciality grains. In*: Cereal grains: properties, processing, and nutritional attributes*. Pp. 43–80. Boca Raton: CRC Press

Singh CB, Jayas DS, Paliwal J, White NDG (2010) Identification of insect-damaged wheat kernels using short-wave near-infrared hyperspectral and digital colour imaging. Comput Electron Agric 73(2):118–125

Vermeulen P, Ebene M, Orlando B, Fernández Pierna J, Baeten V (2017a) Online detection and quantification of particles of ergot bodies in cereal flour using near-infrared hyperspectral imaging. Food Addit Contam: Part A 34(8):1312–1319

Vermeulen P, Flémal P, Pigeon O, Dardenne P, Fernández Pierna J, Baeten V (2017b) Assessment of pesticide coating on cereal seeds by near infrared hyperspectral imaging. J Spect Imaging 6:1–7

Wang L, Liu D, Pu H, Sun DW, Gao W, Xiong Z (2014) Use of hyperspectral imaging to discriminate the variety and quality of Rice. Food Anal Methods 8(2):515–552

Wang L, Sun DW, Pu H, Zhu Z (2015) Application of hyperspectral imaging to discriminate the variety of maize seeds. Food Anal Methods 9(1):1–10

Weinstock BA, Janni J, Hagen L, Wright S (2006) Prediction of oil and oleic acid concentrations in individual corn (*Zea mays* L.*)* kernels using near-infrared reflectance hyperspectral imaging and multivariate analysis. Appl Spectrosc 60(1):9–16

Williams PJ, Kucheryavskiy S (2016) Classification of maize kernels using NIR hyperspectral imaging. Food Chem 209:131–138

Williams P, Geladi P, Fox G, Manley M (2009) Maize kernel hardness classification by near infrared (NIR) hyperspectral imaging and multivariate data analysis. Anal Chim Acta 653(2):121–130

Williams PJ, Geladi P, Britz TJ, Manley M (2012) Investigation of fungal development in maize kernels using NIR hyperspectral imaging and multivariate data analysis. J Cereal Sci 55(3):272–278